

Supporting Information

Methods

AFM characterization of PDA chip surface. An atomic force microscopy (AFM, Dimension Icon, Bruker) was also employed to analyze the topography of the silicon surface with different concentrations of PDA. The AFM images were acquired in the tapping mode on a $5.0 \mu\text{m} \times 5.0 \mu\text{m}$ scan area.

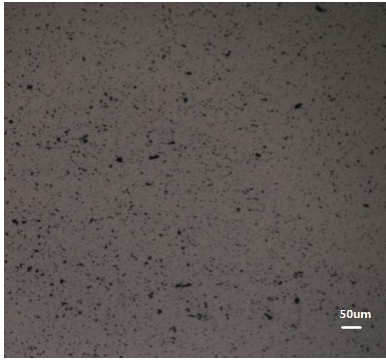
The quantification method of the proteins encapsulated in PDA layer. The glass chip was modified with different concentrations of dopamine (16.5mM, 33mM, 66mM). And then HRP with different concentrations (5, 10, 50mg/ml) was mixed with dopamine for encapsulation and reacted for 1 hour. After wash slides with deionized water 2~3 times, dry in 37°C , the glass slides were assembled in FAST FRAM module (Sigma-Aldrich, United States.), and then 100ul TMB substrate was added into each array and followed by shaking for 25 minutes in 25°C in the dark. At last, 50ul TMB stop solution was added into each array, followed by shaking for about 5 minutes in 25°C and the color of the solution changes from blue to yellow. The UV absorption of each array solution was recorded at 450 nm with microplate reader within 30 minutes.

Characterization of Exosomes by TEM, NTA, Zeta potential analysis. About $10 \mu\text{L}$ exosomes solution diluted in proper proportion was dropped on the 400-mesh Copper-carbon grids (YaSheng Electronic Technology Company, Beijing, China) and immediately scanned under the transmission electron microscope (TEM) after drying for about 10mins. After filtrating through 0.22 μm filter, 1mL exosome solution diluted 50 folds for Nanosight Tracking Analysis (NTA) test was analyzed in Nanosight NS300 (Malvern Company, England). The main parameters were as following: laser type was Blue488, camera level was 13, detection threshold was 3, the temperature was 22.9 to 23.1°C , syringe pump speed was 30. This nanoparticles-calculated experiment was repeated for five times to number the exosomes (<200nm), the final result was the average. For the Zeta potential analysis, the original solution was diluted in water in ratio of 1:10(PBS:water), then about 1mL diluted sample was tested by Zetasizer Nano(ZS90, England, Malvern Instruments). The system repeated the particle-counting process for five times and averaged the data. The size and concentration of exosomes were showed in the formation of Mean \pm Standard Deviation.

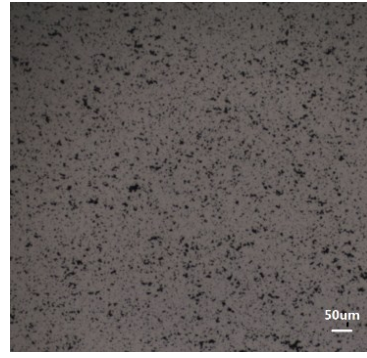
Flow Cytometry. The exosomes from PANC-01 and HPDE6-C7 cell lines were captured by SM3-P100 magnetic beads with anti-CD9/CD63/MIF/GPC-1 respectively. In detail, about $200 \mu\text{L}$ SM3-P100 superparamagnetic nanoparticle solution (10mg/mL) was added into 2.0 mL Microfuge Tubes, then it was watered by $500 \mu\text{L}$ MEST (10mM MES solution with 0.05% Tween® 20) and magnetically separated to delete the supernatant for three times. About $200 \mu\text{L}$ EDC (5mg/mL EDC in 10mM MES solution) and $200 \mu\text{L}$ NHS (5mg/mL NHS in 10mM MES solution) were added into the precipitation, then it was shaking at 37°C for 30mins for magnetic bead activation. After activation, the magnetic beads were diluted into appropriated concentration with PBS and divided into each examined tubes, then about 40ug anti-CD9/CD63/MIF/GPC-1 was added separately and rotated 360 degrees at 37°C for 3 hours for coupling reaction in Tilting vortex mixer(IKA, German, 0004006000). The antibody-magnetic beads were separated magnetically and suspended with PBST (0.02% BSA, 0.05% Tween® 20) in suitable volume and rotated at 37°C for 30mins, then it was watered by PBST as above for three times. After that, a proper

amount of exosomes was added and the tube was rotated 360 degrees at 37°C for 1 hours, subsequently the magnetic beads were separated and watered by PBS for three times. Finally, 1 mL 30 μ M Dio in ethanol was added into each tube and rotated at 37°C for 30mins, then the magnetic beads-exosome complexes were separated and resuspended in PBS in proper concentration for the following flow cytometry (Beckman Coulter, United States, Gallios). Both PANC-01 and HPDE6-C7 groups had the controlled samples with goat anti-mouse IgG instead of anti-CD9/CD63/MIF/GPC-1. Analysis software was Flow Jo 7.6. The percentage of anti-CD9/CD63/MIF/GPC-1 positive exosomes was investigated in about 100000 events. Excitation wavelength was 484 nm, emission wavelength was 501 nm.

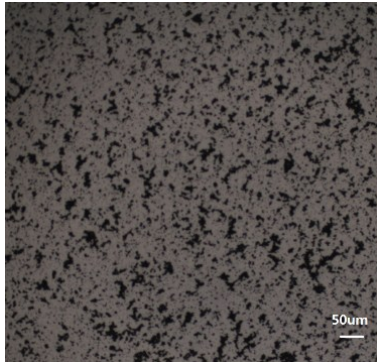
a)



16.5mM dopamine

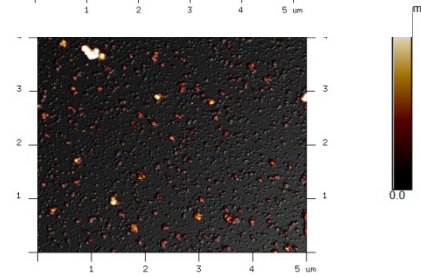
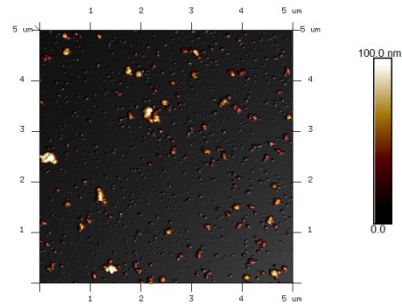
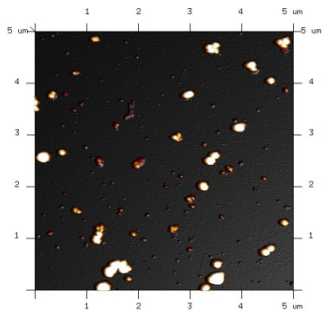


33mM dopamine

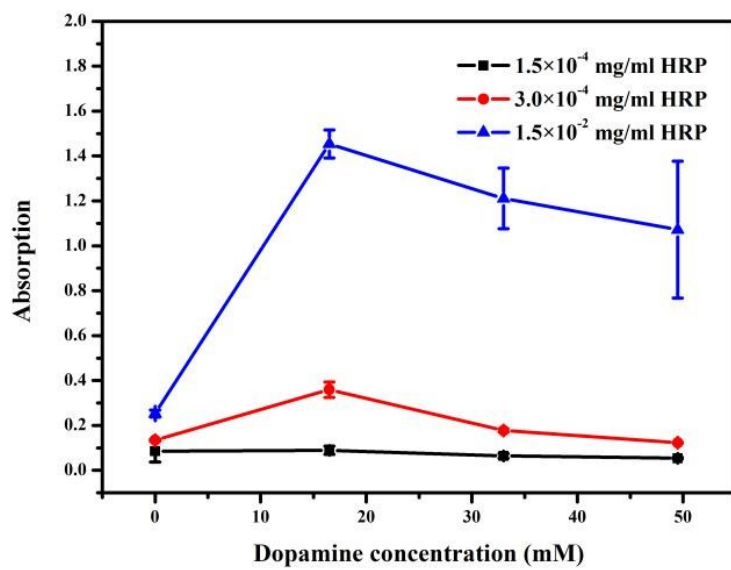


66mM dopamine

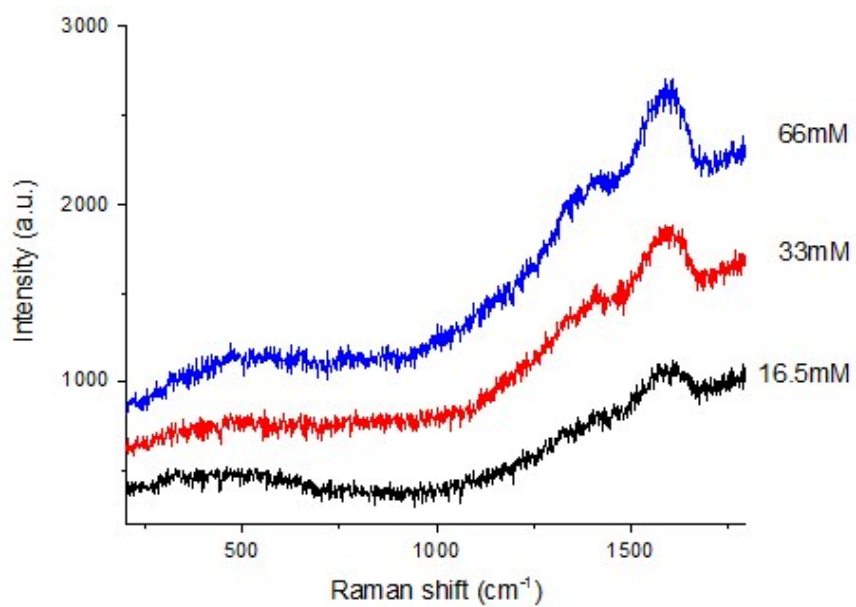
(b)



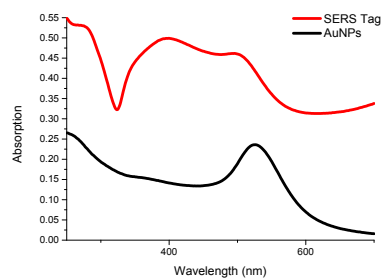
(c)



(d)



(e)



(f)

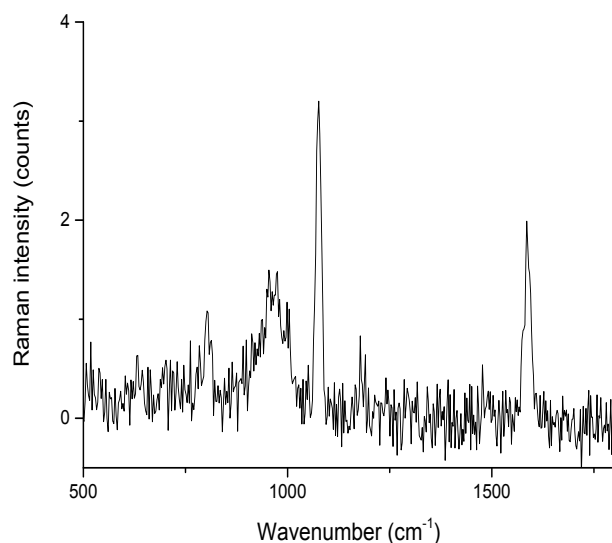


Figure S1 (a) The microscopy images and (b) AFM images of polydopamine chips formed by different dopamine concentrations (16.5mM, 33mM, 66mM). (c). The absorption of TMB catalyzed by HRP encapsulated with polymerization of different concentrations of dopamine (16.5mM, 33mM, 66mM). (d) Raman spectrum of different concentration dopamine polymerized glass slide (the acquisition time of the three spectrum is 100s). e) UV-vis absorbance spectra of Au NPs (black line) and SERS Tags (red lines). f) SERS spectra of SERS Tag solution acquired under low laser power (0.05mW) and short acquisition time (10ms averaged for 100 times).

Obvious differences can be observed from the UV visible absorption spectra of gold nanoparticles and SERS tag. Gold nanoparticles (black line) have only one absorption peak at 521nm, while SERS tag appears two distinct absorption peaks at about 400nm and 500nm, which were attributed to the absorption peaks of the silver layer and the gold nanoparticles respectively.

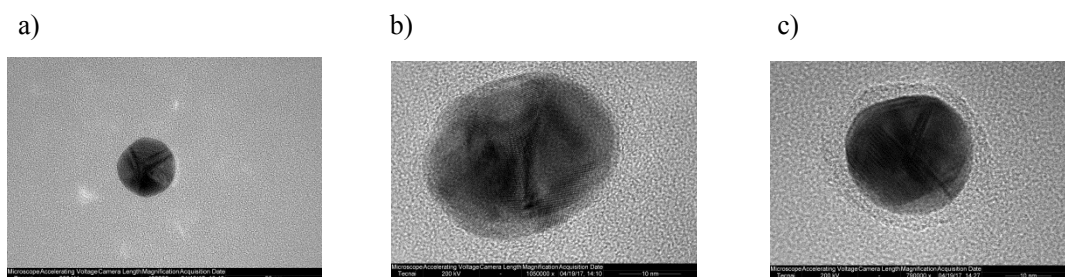


Figure S2. TEM image of a) AuNPs, b) Au@Ag NPs, c) SERS Tag
The high resolution TEM image showed that AuNPs, Au@Ag NPs and SERS Tag have different appearance (Fig.S2).

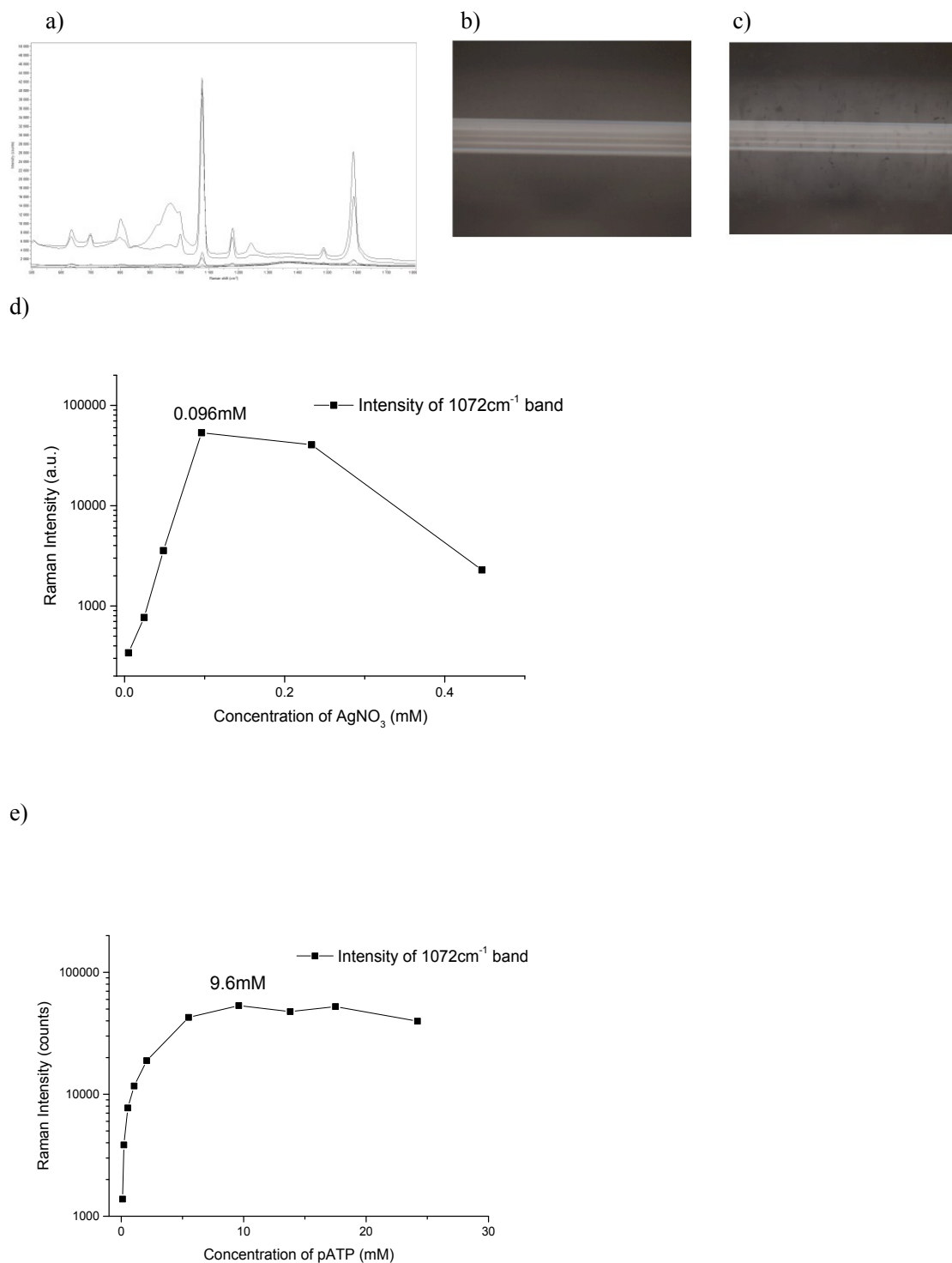


Figure S3. a) SERS spectrum of different concentration AgNO₃ reacted Au@Ag NPs with 100 μ L 10⁻⁴M pATP. b) Digital image of SERS Tag solution with 0.096mM AgNO₃ in capillary. c) Digital image of SERS Tag solution with 0.23mM AgNO₃ in capillary. d) Influence of AgNO₃ volume on SERS intensity. e) Influence of PATP volume on SERS intensity.

Except for the dopamine thickness, the thickness of Ag shell and the concentration of SERS reporter molecular also influence the signal and stability of SERS probe. Fig. S3 show the influence of the AgNO₃ amount on SERS intensity, it is found that the intensity of 1072cm⁻¹ band

significant increased when the AgNO_3 concentration increase from 0.004mM to 0.455mM, because that the thicker Ag shell could promote the Enhance Factor (EF) of NPs. When the AgNO_3 concentration exceeds 0.096mM, the Raman intensity dramatically dropped because of the aggregation of the NPs. The SERS Tag solution with 0.23mM AgNO_3 solution still maintains stable, however, big aggregations were observed in the solution with 1mM AgNO_3 (Fig. S3 b and c). The concentration of Raman reporter molecular attached on the NPs is another principal factor which influences on the SERS intensity and stability of the SERS Tag. As shown in Fig.S3e, when the concentration of *p*ATP was increased to 9.6mM, SERS intensity increased dramatically, but once the concentration exceeded 9.6mM, the intensity maintained at a same level or dropped slightly. Moreover when *p*ATP concentration was 9.6mM, the solution with *p*ATP concentration still maintain clear without aggregation. Based on these results, the optimized concentration of AgNO_3 and *p*ATP were chosen as 0.23mM and 9.6mM respectively to achieve the highest Raman signal intensity and good stability of SERS Tag solution.

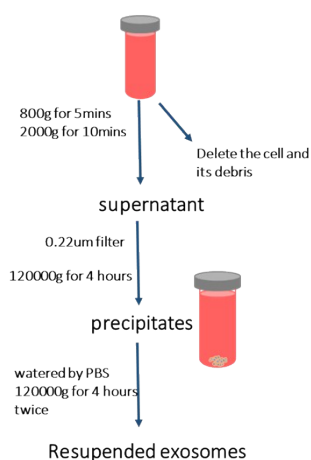
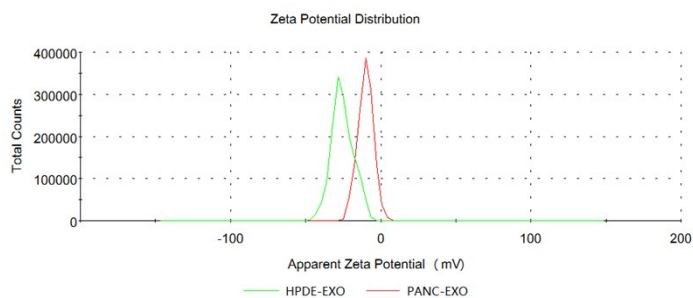


Figure S4 The scheme of the ultracentrifuge processes to separate exosomes from the cell culture medium

a)



b)

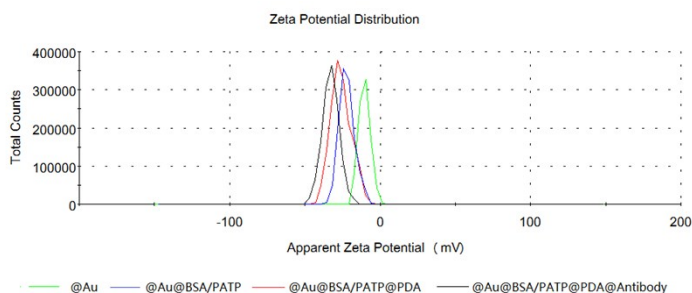
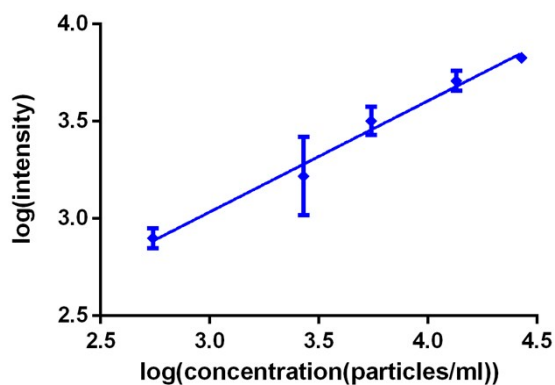
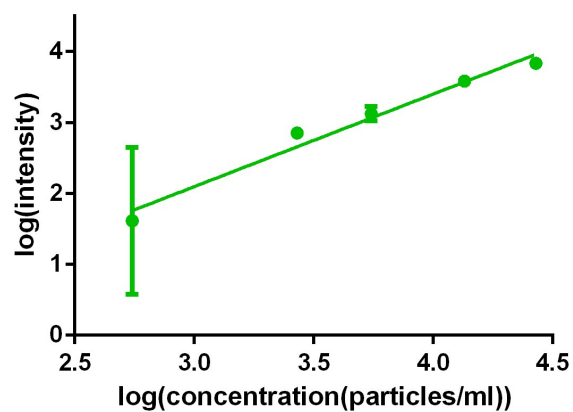


Figure S5 (a) The Zeta potential of HPDE6-C7-exosomes(-25.4mV) and PANC-01-exosome(-10.1 mV). (b) The Zeta potential of Au (-10.3mV), Au@BSA(-22.2mV), Au@BSA@PDA(-26.0 mV), Au@BSA@PDA@antibody(-32.8 mV) . The zeta potential of HPDE6-C7-exosomes was - 25.4mV while PANC-01-exosome was -10.1 mV, which may be resulted from the different compositions of biological molecules (such as proteins) on the exosomes surface of the two cell lines.

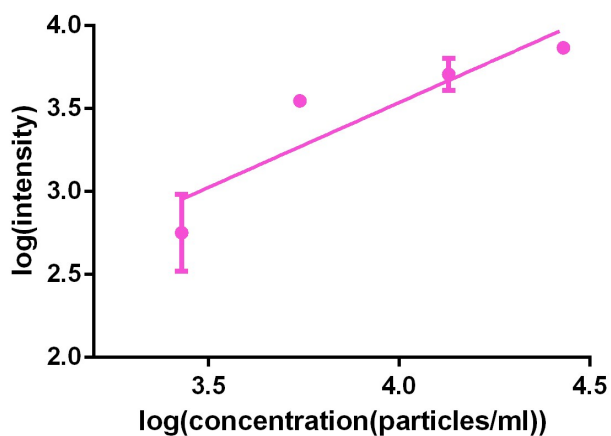
a)



b)



c)



d)

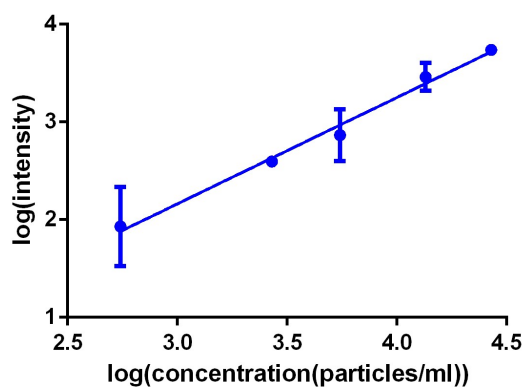


Figure S6 (a) the linear relationship between the SERS intensity with different PANC-01 exosome concentration from 5.44×10^2 to 2.72×10^4 particles/mL in the anti-GPC1 group (b) the linear relationship between the SERS intensity with different PANC-01 exosome concentration from 5.44×10^2 to 2.72×10^4 particles/mL in the anti-EGFR group (c) the linear relationship between the SERS intensity for CD63 with different PANC-01 exosome concentration from 2.72×10^3 to 2.72×10^4 particles/mL (d) the linear relationship between the SERS intensity for EpCAM with different PANC-01 exosome concentration from 5.44×10^2 to 2.72×10^4 particles/mL.

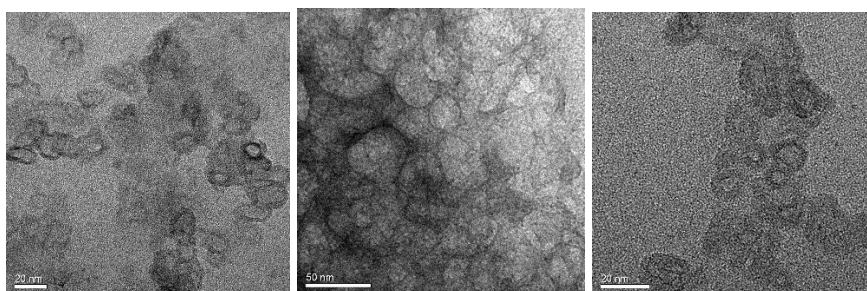


Figure S7 The TEM images of exosomes from serum of patients with pancreatic cancer.

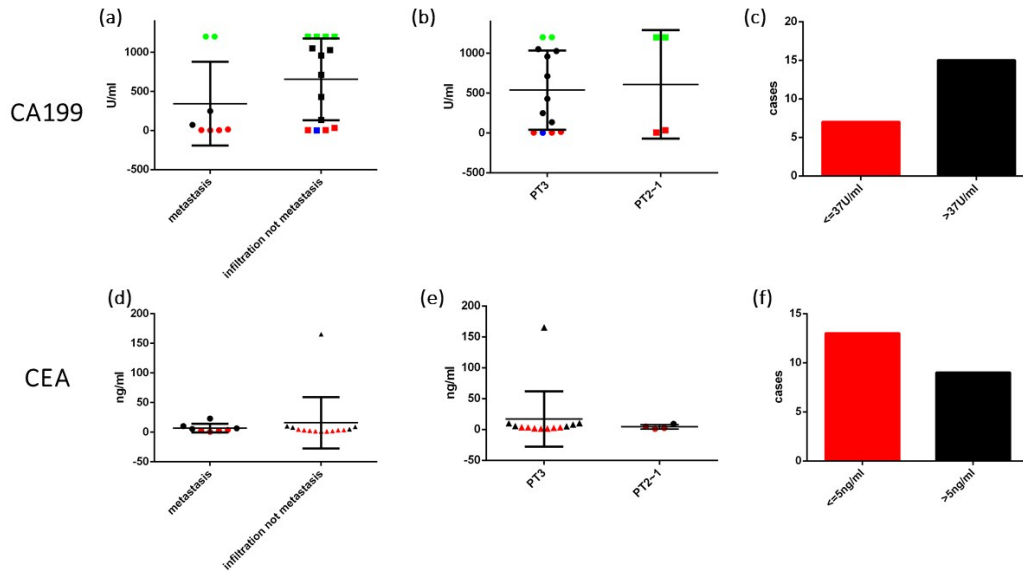


Figure S8 The clinical values of CA19-9 and CEA in serum samples from patients with pancreatic cancer. Note: the red points represented the samples below the clinical reference value. In (d-a), (d-b) the green spots represented that the values was more than 1200 U/mL, while the blue one represented that the value was less than 2U/mL which was also the point that was below the clinical reference value.

We also investigated the clinical ELISA data of two standardized cancer markers, CEA and CA19-9, of these pancreatic cancer patients (n=22). The clinical reference value of CA19-9 was 37U/mL. For these 22 serum samples from pancreatic cancer patients, there were 7 cases below 37U/mL and 15 cases above 37U/mL (Fig. S8-a,c). The Mann-Whitney test for CA19-9 values (the results >1200U/mL was regarded as 1200U/mL, the results <2U/mL was regarded as 2U/mL) of “metastasis” and “infiltration not metastasis” groups showed that $Z=-1.103$, $P=0.270$, for PT3 and PT1~2 subgroups, the results showed that $Z=-0.570$, $P=0.569$ (Fig. 6C-b). While for CEA, the clinical reference value was 5ng/mL, there were 13 cases below 5ng/mL and 9 cases above 5ng/mL (Fig. S8-d, f). The Mann-Whitney test for CEA values of “metastasis” and “infiltration not metastasis” groups showed that $Z=-0.478$, $P=0.6333$, for PT3 and PT1~2 subgroups, the results showed that $Z=-0.566$, $P=0.571$ (Fig.S8-e). The results indicated that both CA19-9 and CEA had high false negative results and could not distinguish the two pairs of subgroups as MIF-exosome-SERS platform did.

Table S1. Linear fitting equation, R value, P value and LOD of five different antibody SERS immunosensor

Antibody	Linear fitting equation	R value ^a	P value ^b	LOD (mol/L)
Anti-MIF	$y = -2.4152 + 1.2392x$	0.99736	1.63094×10^{-4} (<0.05)	9×10^{-19}
Anti-GPC1	$y = 1.34396 + 0.56688x$	0.99542	3.71937×10^{-4} (<0.05)	9×10^{-19}
Anti-EGFR	$y = -0.2903 + 0.92853x$	0.99738	1.60697×10^{-4} (<0.05)	9×10^{-19}
Anti-CD63	$y = -0.43503 + 0.99543x$	0.91115	0.08885 (>0.05)	4.5×10^{-18}
Anti-EpCAM	$y = -0.87148 + 1.03588x$	0.9937	5.99785×10^{-4} (<0.05)	9×10^{-19}

^a Multiple correlation coefficient; ^b Probability, >0.05 means without statistical difference.

Table S2 The information of the patients diagnosed as pancreatic cancer histologically.

Patient No.	Age (Years)	Gender (F/M)	TNM Stage	Infiltrated Nearby Organs and Metastasis	Histopathological report
1	46	F	-	metastasizing to the liver	Low differentiated pancreatic head ductal adenocarcinoma
2	68	F	-	metastasizing to the liver	Low differentiated pancreatic head malignant tumor
3	68	M	PT3N1Mx	duodenal submucosal layer	Moderated to low differentiated pancreatic head ductal adenocarcinoma, invading adipose tissue around the of the pancreas, nerve invasion(+), tumor emboli within the vessels(+)
4	60	F	-	metastasizing to the liver	Pancreatic space occupying lesion, Low differentiated pancreatic malignant tumor
5	71	M	PT3N3Mx	-	Moderated to low differentiated pancreatic head ductal adenocarcinoma, invading adipose tissue around the of the pancreas, nerve invasion(+)
6	52	M	-	metastasizing to hilum of spleen	Pancreatic body-tail neuroendocrine tumor, invading adipose tissue around the pancreas
7	57	M	-	Widely metastasizing to the peritoneum	Pancreatic body malignant tumor
8	66	M	PT3N1Mx	Metastasizing to The adrenal glands	Moderate differentiated pancreatic body-tail ductal adenocarcinoma, invading adipose tissue and lymph codes around the pancreas, nerve invasion(+)
9	73	M	PT3N1Mx	Lymph code Metastasis	Moderate differentiated pancreatic head ductal adenocarcinoma, nerve invasion(+), invading adipose tissue and lymph codes(1/1)
10	63	F	PT3N1Mx	omentum majus(1/4)	Moderated to low differentiated pancreatic ductal adenocarcinoma, invading adipose tissue around the of the pancreas, nerve invasion(+)
11	40	M	PT3N1bMx	Common bile duct and main pancreatic duct, Lymph code Metastasis	Low differentiated pancreatic ductal adenocarcinoma, nerve invasion(+), invading adipose tissue and lymph codes(15/16) around the pancreas
12	64	F	PT3N0Mx	duodenal submucosal layer, Bile duct	The pancreas intraductal papillary mucinous tumor with invasive carcinoma, invading adipose tissue around the of the pancreas, nerve invasion(+)
13	62	M	PT3N1M1	-	low differentiated pancreatic ductal adenocarcinoma, local mucinous non-cystic carcinoma, invading adipose tissue around the of the pancreas, the pancreas cut edge and lymph codes, nerve invasion(+), tumor emboli within the vessels(+)
14	40	M	PT3N0Mx	Duodenum, bile duct	Moderated differentiated pancreatic head ductal adenocarcinoma, invading adipose tissue around the of the pancreas, nerve invasion(+)
15	53	M	PT3N0Mx	The duodenum muscle layer	Moderated differentiated pancreatic body-tail ductal adenocarcinoma, invading adipose tissue around the of the pancreas, nerve invasion(+)
16	74	F	PT3N0Mx	-	Moderated to low differentiated pancreatic head ductal adenocarcinoma. Chronic cholecystitis.
17	69	M	PT3N0Mx	-	Low differentiated pancreatic body-tail ductal adenocarcinoma, invading adipose tissue around the of the pancreas, nerve invasion(+)
18	53	F	PT3N1Mx	duodenal submucosal layer, bile duct	Moderate differentiated pancreatic head ductal adenocarcinoma, nerve invasion(+), invading adipose tissue and lymph codes around the of the pancreas
19	56	M	PT2N1aMx	-	Moderate differentiated pancreatic head ductal adenocarcinoma, invading adipose tissue and lymph codes around the of the pancreas
20	65	F	PT2N0Mx	-	Moderate differentiated pancreatic head ductal adenocarcinoma, nerve invasion(+)
21	63	F	PT2N0Mx	-	Moderate differentiated pancreatic head ductal adenocarcinoma, nerve invasion(+)
22	67	M	PT1N0Mx	-	Moderate differentiated pancreatic head ductal adenocarcinoma, nerve invasion(+)
23	62	M	PT3N1M1	Invade nerve and peripancreatic adipose tissue	Pancreatic body malignant tumor, abdominal aortic aneurysm and atherosclerosis
24	79	M	-	-	Intraductal papillary mucinous tumors of the pancreas, hypertension, arrhythmia and sinus bradycardia
25	76	M	PT3N1Mx	-	Invade duodenal mucosa and pancreatic fat, nerve invasion(+), invading adipose tissue and lymph codes
26	75	F	PT3N0Mx	Invade nerve	Malignant neoplasm of head of pancreas and hepatic cyst

27	75	M	PT3N1Mx	The duodenum muscle layer	Middle differentiated ductal adenocarcinoma of the pancreas, chronic cholecystitis and hypertension
28	73	F	PT3N1Mx	-	Pancreatic space occupying lesion, hepatic cyst, after subtotal gastrectomy
29	72	F	PT3N1Mx	lymph nodes around stomach	Chronic hepatitis B, chronic congestion of spleen
30	72	F	PT3N0Mx	-	Diabetes, hypothyroidism, cholecolithiasis and chronic cholecystitis and gallbladder stone
31	71	M	PT3N0Mx	Common bile duct	acute pancreatitis, cirrhosis, gallstone
32	70	F	PT3N0Mx	-	Chronic splenic congestion, chronic cholecystitis
33	69	M	PT3NxMx	-	Malignant tumor of pancreatic tail, squamous cell carcinoma of pancreatic tail, hypertension, arrhythmia, old myocardial infarction and type-2 diabetes
34	69	M	PT3NxMx	-	Malignant tumor of pancreatic tail, squamous cell carcinoma of pancreatic tail, hypertension, arrhythmia, old myocardial infarction and type-2 diabetes
35	69	F	-	Omentum majus	Pancreas occupying and type-2 diabetes
36	68	M	-	Metastasis of liver	Carcinoma of neck of pancreas with metastasis of liver and hypertension
37	68	M	-	-	malignant pancreatic tumor, secondary pancreatitis, hypertension, diabetes and hyperlipidemia
38	67	F	-	-	Hypertension and mucinous cystadenoma of the head of pancreas
39	66	M	-	-	Malignant neoplasm of head of pancreas and hypertension, infiltrating adjacent fat
40	66	M	-	-	Pancreatic head tumor and chronic cholecystitis
41	66	M	PT3N0Mx	The duodenum muscle layer	Malignant neoplasm of head of pancreas, hypertension, type-2 diabetes, nerve invasion(+)
42	66	F	-	Cystic duct	malignant pancreatic tumor, hypertension and type-2 diabetes, nerve invasion(+)
43	66	M	-	Common bile duct	Malignant tumor, jaundice obstructive, hypertension and prostatic hyperplasia
44	66	F	PT3N0Mx	-	Malignant neoplasm of neck of pancreas
45	65	F	PT3N0Mx	Lymph node metastasis	Hypertension, Infiltrating of peripancreatic fat and Lymph node metastasis, nerve invasion(+)
46	65	M	-	-	Pancreatic space occupying lesion, hypertension and diabetes
47	64	M	PT3N2Mx	The duodenum muscle layer	Malignant neoplasm of head of pancreas and hypertension, nerve invasion(+)
48	64	M	-	-	Chronic pancreatitis of pancreas head
49	64	F	-	Omentum majus	Malignant tumor of pancreatic tail
50	64	M	PT3N1Mx	The duodenum muscle layer	Viral hepatitis B, prostatic hyperplasia and ductal adenocarcinoma of the head of pancreas
51	60	M	PT3N0Mx	-	Adenocarcinoma of pancreatic duct, chronic congestion of spleen and nerve invasion(+)
52	59	F	PT3N0Mx	-	Malignant neoplasm of body and tail of pancreas, coronary heart disease, hypertension and chronic congestion of spleen
53	58	M	PT3N0Mx	-	chronic congestion of spleen and chronic cholecystitis
54	58	M	-	omentum	Malignant neoplasm of pancreatic body and hypertension
55	57	M	PT3N0Mx	Duodenal cystic duct	Middle differentiated ductal adenocarcinoma of the pancreas, hypertension and nerve invasion(+)
56	56	M	PT3N0Mx	-	chronic cholecystitis, type-2 diabetes, hypertension, nerve invasion(+)
57	56	M	-	-	chronic cholecystitis, hypertension, chronic congestion of spleen, lower limbs varicosity medication
58	56	F	PT3N0Mx	-	Ductal carcinoma of the body and tail of pancreas, hypertension, chronic congestion of spleen and nerve invasion(+)
59	56	F	PT3N1Mx	-	Carcinoma of body and tail of pancreas, type-2 diabetes, chronic congestion of spleen and nerve invasion(+)
60	52	F	-	-	Tumor of body and tail of pancreas, hypertension and chronic cholecystitis
61	49	M	PT3N0Mx	-	chronic congestion of spleen, nerve invasion(+)
62	48	F	-	The duodenum muscle layer and gallbladder	chronic cholecystitis and nerve invasion(+)
63	48	F	-	-	Neuroendocrine carcinoma of pancreas
64	46	M	-	-	chronic pancreatitis, malignant neoplasm of head of pancreas and viral hepatitis B
65	43	F	-	-	chronic congestion of spleen
66	41	F	-	-	Solid pseudopapillary tumor and vascular invasion
67	41	F	-	-	Solid pseudopapillary tumor, chronic congestion of spleen
68	40	M	-	-	Jaundice obstructive and carcinoma of head of pancreas
69	29	F	-	-	Serous cystadenocarcinoma of pancreatic head
70	25	F	-	-	Malignant neoplasm of neck of pancreas
71	59	F	-	-	Malignant neoplasm of body and tail of pancreas, coronary heart disease, old myocardial infarction, hypertensive disease

Note: F, female; M, male; TNM:T, tumor, N, node, M, metastasis

Table S3. The statistical results of MIF platform

MIF	Cancer	P3	Metastasis
$W_{\text{control}}=0.806, P<0.0001^a$; $W_{\text{experiment}}=0.916, P<0.0001^a$; $F=314.177, P<0.0001^b$			
Healthy	$Z=-6.257, P<0.0001^c$		
P1~2		$Z=-3.207, P=0.001^c$	
Non metastasis			$Z=-2.736, P=0.006^c$

^a Shapiro-Wilk test values; ^bLevene's test for equality of variances; ^c Mann-Whitney test values.

Table S4 The statistical results of GPC1 platform

GPC1	Cancer	P3	Metastasis
$W_{\text{control}}=0.778, P<0.0001^a$; $W_{\text{experiment}}=0.934, P=0.041^a$; $F=36.372, P<0.0001^b$			
Normal	$Z=-2.425, P=0.015^c$		
P1~2		$Z=-0.189, P=0.850^c$	
Non metastasis			$Z=-1.034, P=0.301^c$

^a Shapiro-Wilk test values; ^bLevene's test for equality of variances; ^c Mann-Whitney test values.

Table. S5 The statistical results of EGFR platform

EGFR $W_{\text{control}}=0.828, P<0.0001^a$; $W_{\text{experiment}}=0.880, P=0.001^a$; $F=54.973, P<0.0001^b$	Cancer	P3	Metastasis
Normal	$Z=-1.7962, P=0.072^c$		
P1~2		$Z=-1.701, P=0.089^c$	
Non metastasis			$Z=-0.293, P=0.770^c$

^a Shapiro-Wilk test values; ^bLevene's test for equality of variances; ^c Mann-Whitney test values.